UNIVERSITY OF AMSTERDAM

UvA-DARE (Digital Academic Repository)

Revisiting Multizone Jet Models Applied to the Quiescent Black Hole X-Ray Binary XTE J1118+480

Clapp, Octavia D.; Plotkin, Richard M.; Lucchini, Matteo; Markoff, Sera; Gallo, Elena; Zuo, Zihao

DOI
10.3847/1538-4357/ae47f1

Publication date
2026

Document Version
Final published version

Published in
Astrophysical Journal

License
CC BY

Link to publication

Citation for published version (APA):
Clapp, O. D., Plotkin, R. M., Lucchini, M., Markoff, S., Gallo, E., & Zuo, Z. (2026). Revisiting Multizone Jet Models Applied to the Quiescent Black Hole X-Ray Binary XTE J1118+480. *Astrophysical Journal*, *1000*(2), Article 278. https://doi.org/10.3847/1538-4357/ae47f1

General rights
It is not permitted to download or to forward/distribute the text or part of it without the consent of the author(s) and/or copyright holder(s), other than for strictly personal, individual use, unless the work is under an open content license (like Creative Commons).

Disclaimer/Complaints regulations
If you believe that digital publication of certain material infringes any of your rights or (privacy) interests, please let the Library know, stating your reasons. In case of a legitimate complaint, the Library will make the material inaccessible and/or remove it from the website. Please Ask the Library: https://uba.uva.nl/en/contact, or a letter to: Library of the University of Amsterdam, Secretariat, P.O. Box 19185, 1000 GD Amsterdam, The Netherlands. You will be contacted as soon as possible.
UvA-DARE is a service provided by the library of the University of Amsterdam (https://dare.uva.nl)

Download date:09 Nov 2026

The Astrophysical Journal, 1000:278 (9pp), 2026 April 1 https://doi.org/10.3847/1538-4357/ae47f1
© 2026. The Author(s). Published by the American Astronomical Society.
OPEN ACCESS

Revisiting Multizone Jet Models Applied to the Quiescent Black Hole X-Ray Binary XTE J1118+480

Octavia D. Clapp[1], Richard M. Plotkin[1,2], Matteo Lucchini[3], Sera Markoff[3,4], Elena Gallo[5], and Zihao Zuo[5]
[1] Department of Physics, University of Nevada, Reno, NV 89557, USA; octavia@umd.edu
[2] Nevada Center for Astrophysics, University of Nevada, Las Vegas, NV 89154, USA
[3] Anton Pannekoek Institute for Astronomy, University of Amsterdam, Science Park 904, 1098 XH Amsterdam, The Netherlands
[4] Gravitational and Astroparticle Physics Amsterdam, University of Amsterdam, Science Park 904, 1098 XH Amsterdam, The Netherlands
[5] Department of Astronomy, University of Michigan, 1085 South University, Ann Arbor, MI 48109, USA
Received 2025 July 11; revised 2026 January 22; accepted 2026 February 17; published 2026 March 27

Abstract

Black hole X-ray binaries are capable of launching compact radio jets, even in their quiescent state where they spend the majority of their time accreting at low Eddington ratios $L_X/L_{Edd} \lesssim 10^{-5}$. There are still several open questions regarding the physical properties of quiescent black hole jets and accretion flows. Here, we apply a steady-state multizone jet model (`BHJet`) to the broadband spectrum of the highly quiescent black hole X-ray binary XTE J1118+480 ($L_X/L_{Edd} \sim 10^{-8.5}$), and we compare our results to previous work that applied a predecessor model to the same broadband spectrum. We find two statistically comparable model fits that explain the X-ray emission as either synchrotron self-Compton (from a thermal distribution of particles in the jet base) or as synchrotron-cooled radiation (from an accelerated tail of nonthermal particles). However, we argue that the synchrotron self-Compton fit is more realistic. Finally, we confirm previous suggestions that the jet base becomes cooler and more compact in quiescence, compared to hard state black hole X-ray binaries.

Unified Astronomy Thesaurus concepts: X-ray binary stars (1811); Black hole physics (159); Astronomy data modeling (1859); Relativistic jets (1390)

1. Introduction

Black hole X-ray binaries (BHXRBs) contain an $\sim 10\,M_\odot$ black hole accreting material from a companion star. They are among the most powerful multiwavelength emitters within galaxies and are also multimessenger sources of cosmic rays (LHAASO Collaboration et al. 2025; H. Yue et al. 2026). Some BHXRBs, particularly ones with low-mass companion stars, undergo outburst cycles where they brighten by orders of magnitude (typically reaching X-ray luminosities $L_X \sim 0.1 L_{Edd}$, where $L_{Edd} = 1.3 \times 10^{39}$ erg s^{-1} is the Eddington luminosity for a $10\,M_\odot$ black hole). In the canonical picture, transient BHXRBs undergo state transitions that reflect changes in the structure of the underlying accretion flow (R. A. Remillard & J. E. McClintock 2006; T. M. Belloni & S. E. Motta 2016). As BHXRBs progress through outbursts, radio campaigns have shown that compact relativistic outflows (i.e., compact jets) are present toward the beginnings and ends of outbursts in the "hard state" (referring to a hard X-ray spectrum, indicative of nonthermal radiative processes). Meanwhile, compact jets are quenched when outbursting systems transition into a "soft state," where X-ray emission is produced by thermal emission from a multitemperature accretion disk (N. I. Shakura & R. A. Sunyaev 1973). See R. Fender (2010) for an overview of radio phenomenology.

Similar to supermassive black holes, BHXRBs spend most of their time in a "quiescent" spectral state, where they emit much lower luminosities (following R. M. Plotkin et al. 2013, we define quiescence as $L_X \lesssim 10^{-5} L_{Edd}$). Even though quiescence is the most common accretion state, it is arguably the least understood, largely because the low luminosities dictate that decent quality datasets can be obtained only for the closest systems. Nevertheless, there is agreement that quiescent BHXRBs accrete from some version of a radiatively inefficient accretion flow (RIAF). In an RIAF, the inner flow becomes geometrically thick and transforms into a two-temperature plasma that emits less radiation compared to a standard geometrically thin disk (S. Ichimaru 1977; R. Narayan & I. Yi 1994, 1995; F. Yuan & R. Narayan 2014). Observationally, quiescent BHXRBs have softer X-ray spectra compared to hard state BHXRBs (X-ray photon indices $\Gamma \approx 2.1$ in quiescence versus ≈ 1.5 in the hard state; A. K. H. Kong et al. 2002; S. Corbel et al. 2006; R. M. Plotkin et al. 2013; M. T. Reynolds et al. 2014). Compact jets also persist into quiescence, based on radio detections of around a half-dozen different quiescent systems (E. Gallo et al. 2005, 2006, 2014; S. Corbel et al. 2013; S. A. Dzib et al. 2015; M. Ribó et al. 2017; E. Tremou et al. 2020; R. M. Plotkin et al. 2021; F. Carotenuto et al. 2022).

The detailed natures of quiescent accretion flows and jets are still under debate, however. For example, softer X-ray emission could be a result of lower densities in the accretion flow (which yield a lower optical depth to inverse-Compton scattering and/or a more dominant emission component from bremsstrahlung radiation; A. A. Esin et al. 1997). Or, the softer X-ray spectra could reflect changes in relativistic jet properties, such as the distribution of nonthermal particles steepening with decreasing accretion rate (S. Markoff 2010; R. M. Plotkin et al. 2013).

Further progress requires multiwavelength approaches, but finding appropriate targets is challenging: one must coordinate multiple facilities to observe sources that, even for our largest telescopes, are typically close to detection limits. Moreover, because broadband emission is variable even in quiescence,

Original content from this work may be used under the terms of the Creative Commons Attribution 4.0 licence. Any further distribution of this work must maintain attribution to the author(s) and the title of the work, journal citation and DOI.

coordination of these facilities must occur within 1–2 days (R. I. Hynes et al. 2004; F. Bernardini & E. M. Cackett 2014; V. Rana et al. 2016; T. Dinçer et al. 2018; R. M. Plotkin et al. 2019; D. L. dePolo et al. 2022). Essentially, there are only three quiescent systems with nearly simultaneous, well-sampled, broadband spectral energy distributions (SEDs) that include detections in the radio wave band: the relatively luminous quiescent BHXRB V404 Cygni ($L_X \approx 10^{-6} L_{Edd}$; R. I. Hynes et al. 2009; E. S. Borowski et al. 2025), and two systems at lower luminosities ($L_X \approx 10^{-8.5} L_{Edd}$), A0620−00 (E. Gallo et al. 2007; T. Dinçer et al. 2018; Z. Zuo et al. 2025) and XTE J1118+480 (E. Gallo et al. 2014; R. M. Plotkin et al. 2015, hereafter P15). Provided accretion physics is scale invariant, then relative to their Eddington limits, the latter two objects are accreting nearly as weakly as Sgr A* at the center of the Milky Way, making A0620−00 and XTE J1118+480 our two best analogs to (highly) quiescent supermassive black holes.

XTE J1118+480 is a particularly advantageous source for multiwavelength campaigns because it is nearby (only 1.72 kpc away; D. M. Gelino et al. 2006) and located at a high Galactic latitude ($b = +62°$). As such, there is little intervening material along the line of sight, leading to low extinction ($A_V = 0.065$ mag; D. M. Gelino et al. 2006) and column density ($N_H = 1.2 \times 10^{20}$ cm^{-2}; J. E. McClintock et al. 2003). P15 applied a broadband multizone jet model to an SED of XTE J1118+480 in quiescence, which extended from the radio through the X-ray. They noted that the ultraviolet detections of this system were especially constraining, which would not have been possible if the extinction were higher. The broadband modeling of XTE J1118+480 in P15 demonstrated that it is possible to self-consistently explain the full radio through X-ray spectrum by the outflow (plus a near-infrared–optical contribution from the companion star). They additionally found that the relativistic jet base becomes cooler and more compact in quiescence, and possibly less magnetically dominated, compared to fits of the same system using the same jet model when it was 4–5 times more luminous in the hard state (D. Maitra et al. 2009). The above is only one interpretation, however. J. E. McClintock et al. (2003) argued (for a different SED of XTE J1118+480 that did not include radio emission) that high-energy emission can also be explained by the inflow. New JWST observations of a different quiescent source, A0620−00, suggest that outflows in the form of winds are also present (Z. Zuo et al. 2025).

When considering a jet interpretation, P15 suggested that the X-ray emission in quiescence is most likely attributed to synchrotron self-Compton (SSC) radiation, where the seed photons arise primarily from a mildly relativistic thermal distribution of outflowing electrons in the base of the jet. However, they could not exclude an alternative explanation where synchrotron radiation from nonthermal electrons downstream of the jet contribute most of the X-ray emission. R. M. T. Connors et al. (2017) reached a similar conclusion applying a similar jet model to A0620−00 in quiescence, where their fits converged to solutions that could explain X-rays as SSC dominated or as synchrotron dominated (similar to P15, they also found cooler and more compact jet bases in quiescence; also see D. Kantzas & F. Calore 2024). Before attempting to resolve the even murkier question of whether X-rays are emitted mostly by inflowing or outflowing material in quiescence, it would be beneficial to first resolve if the X-ray-emitting particles are primarily thermal or nonthermal.

This paper focuses on improving our understanding of the X-ray emission in an outflow interpretation. P15 adopted the jet model by S. Markoff et al. (2005), which we will refer to as the MNW05 model (also see, e.g., H. Falcke & S. Markoff 2000; S. Markoff et al. 2001, 2003, 2005, 2008; D. Maitra et al. 2009). Over the last decade, additional physics has been incorporated into this model, allowing us to now explore which results from P15 are robust in the context of an outflow model. The newer model, named `BHJet`, was developed by M. Lucchini et al. (2022, hereafter L22) and is available publicly (M. Lucchini et al. 2021a).[6] In particular, `BHJet` includes more sophisticated treatments of radiative processes, and importantly, it tracks how radiative energy losses affect the distributions of radiating electrons (for comparison, the MNW05 model assumes that all energy losses are due to the adiabatic escape of particles along the jet). Furthermore, `BHJet` allows for cyclo-synchrotron radiation (thereby making contributions from mildly relativistic electrons more realistic), and it also includes an improved treatment of inverse-Compton and SSC emission.

In Section 2 we describe the version of the MNW05 model adopted by P15, and we also detail the next-generation `BHJet` model adopted here from L22. We then summarize the observational data and our fitting methods in Section 3. Results are presented in Section 4 and discussed in Section 5. Finally, a summary is provided in Section 6. All uncertainties are reported at the 1σ level.

2. Multizone Jet Models: Comparing MNW05 and `BHJet`

Since our primary goal is to compare results on XTE J1118+480 between the MNW05 model and the newer `BHJet` model, we briefly summarize and compare both models below. Our focus here is on the MNW05 and `BHJet` class of multizone jet models in quiescence, although we refer the reader to several other studies that applied other classes of accretion and jet models to XTE J1118+480 both in quiescence and outburst (e.g., A. A. Esin et al. 2001; J. E. McClintock et al. 2003; J. Malzac et al. 2004; F. Yuan et al. 2005; A. Veledina et al. 2011; G. S. Vila et al. 2012).

2.1. Summary of the MNW05 Model Used by R. M. Plotkin et al. (2015)

We refer the reader to Section 3 of P15 for an overview of the MNW05 model at the time of that publication. Below, we highlight important features relevant to this paper. The model assumes that radiation is leptonic and that kinetic energy is carried by protons. The power injected into the jet is parameterized by a model normalization N_j, which is proportional to the accretion power $\dot{M}_{acc} c^2$, where $\dot{M}_{acc}$ is the mass accretion rate. The model expresses N_j in units of Eddington luminosity. The base of the jet is a cylindrical nozzle with height h_0 and radius r_0.

A free parameter T_e is used to describe the electron temperature of the nozzle, which sets a quasi-thermal, mildly relativistic electron distribution that emits synchrotron radiation and SSC. We note that MNW05 did not include cyclotron processes, so P15 placed a limit for $k_B T_e > 511$ keV (where k_B is the Boltzmann constant). The balance between the energy injected into the magnetic field of the nozzle and into internal

[6] https://github.com/matteolucchini1/BHJet

energies is set by a free parameter $k = U_B/U_e$, where $U_B = B^2/(8\pi)$ is the magnetic energy density (for magnetic field B) and U_e is the electron energy density.[7]

At a distance h_0 from the black hole, the nozzle expands laterally, resulting in a pressure gradient that accelerates plasma along the jet. There is an acceleration zone at a distance $z_{\rm acc}$ from the black hole, at which point a fraction of the particles is accelerated into a nonthermal distribution following a power law with index p (i.e., $N(\gamma) \propto \gamma^{-p}$, where γ is the Lorentz factor), to mimic a collisionless shock. Downstream, these particles produce the characteristic flat and inverted radio spectrum from partial synchrotron self-absorption (R. D. Blandford & A. Königl 1979).

P15 assumed that all energy losses along the jet are dominated by adiabatic losses as particles escape each jet zone, such that the rate of adiabatic escape is $t_{\rm esc}^{-1} = \beta_e c/z$, where $\beta_e c$ is the speed of an electron at a distance z from the black hole. This is balanced by a constant rate of particle acceleration $t_{\rm acc}^{-1} \propto \epsilon_{\rm sc}$, where $\epsilon_{\rm sc}$ is a free parameter that describes (and absorbs uncertainties in) the ratio of the square of the shock velocity and the scattering mean free path relative to the electron gyroradius (see Equation (1) of P15). Finally, P15 represented optical radiation from the companion star by including an additional blackbody component with a temperature of 3400 K, normalized to a star with a radius of $0.56\,R_\odot$ (D. M. Gelino et al. 2006). The best-fit parameters from P15 are provided in Table 1 for convenience.

2.2. Modifications Made in `BHJet` by M. Lucchini et al. (2022)

Here, we focus on additional features in `BHJet` most relevant to our modeling of XTE J1118+480, and we refer the reader to L22 for a full discussion. `BHJet` combines two model flavors, `agnjet` and `bljet`, which allow different assumptions for the jet dynamics. The `agnjet` treatment is, as in MNW05, pressure driven, and `bljet` includes the influence of magnetic fields to the jet outflow dynamics. We attempted to fit both model flavors to XTE J1118+480, but `agnjet` provided better fits (see Section 3), so we focus on `agnjet` here. We refer the reader to L22 for details on `bljet`.

The `agnjet` model can be subdivided into an adiabatic or isothermal version, which refers to how the jet expands and propagates downstream. As discussed in Section 3, our final fits tend to prefer the isothermal version, which we focus on below. L22 warn that the isothermal version does not account for the energy required to reaccelerate particles, for reasons similar to the standard R. D. Blandford & A. Königl (1979) model, which we remain cognizant of in our interpretations.

The inclusion of radiative energy losses is a significant addition in `BHJet`. For convenience, we replicate their Equation (3):

$$\mathring{\varrho}_{\rm rad} = -\frac{4\sigma_{\rm t} c U_{\rm rad}}{3 m_e c^2}\varrho\gamma, \tag{1}$$

where $\varrho = p/(m_e c)$ is a dimensionless momentum, $\mathring{\varrho}_{\rm rad}$ is the momentum loss rate, $\sigma_{\rm t}$ is the Thomson cross section, $U_{\rm rad}$ is the energy density of the radiation field, and γ is the Lorentz factor of the radiating electrons.

[7] We note this equipartition factor k is essentially the inverse of the traditional plasma β parameter for a relativistic lepton gas.

Meanwhile, adiabatic losses, as described by Equation (4) of L22, are parameterized by

$$\mathring{\varrho}_{\rm ad} = -\frac{f_\beta c}{r}\varrho, \tag{2}$$

where r is the radius of the emitting region, and f_β describes a (dimensionless) expansion speed of the emitting region. The parameter f_β essentially absorbs uncertainties in electron diffusion and is a free parameter in the model (f_β was not included in the MWN05 model used by P15). L22 also added cyclo-synchrotron processes, which allow for cooler jet bases, and we lift the constraint $k_{\rm B}T_e > 511$ keV placed by P15.

Finally, for clarity, we comment on some parameters that are redefined in `BHJet` compared to MNW05, and/or that use different nomenclature. First, `BHJet` defines an equipartition parameter at the jet base as $\beta_{\rm p} = U_e/U_B$, while MNW05 adopted the inverse $k = U_B/U_e$. Besides the parameter f_β related to electron diffusion discussed above, a new phenomenological free parameter $f_{\rm pl}$ is introduced that adjusts the temperature profile downstream of the jet (postacceleration zone), which essentially allows one to alter the radio spectral index. For the `agnjet` flavor of `BHJet`, the location of the acceleration zone is denoted by $z_{\rm diss}$ instead of $z_{\rm acc}$. We also note that the parameterization of the blackbody component from the secondary star has changed, where MNW05 set the blackbody normalization through the stellar radius, and `BHJet` sets it through the stellar luminosity. In our analysis using `BHJet` we opted to allow only 10% of particles in the acceleration zone to be accelerated into a nonthermal tail, compared to 60% adopted in P15. A value of 10% appears to be more consistent with expectations regarding mildly relativistic shocks (L. Sironi & A. Spitkovsky 2011; P. Crumley et al. 2019). We also fixed the ratio of height-to-radius ratio of the nozzle to the default $h_0/r_0 = 2$ (compared to 1.5 in MNW05).

3. Analysis

3.1. Archival Data

Our target XTE J1118+480 is a nearby low-mass BHXRB (1.72 ± 0.10 kpc; D. M. Gelino et al. 2006) with an orbital period of $4.08 \pm (5 \times 10^{-6})$ hr (M. A. P. Torres et al. 2004). We adopt the same SED used by P15, and we refer the reader to their Section 2 and Table 1 for a full description of their data. Briefly, nearly simultaneous observations were taken from 2013 June 27 to 28 with the Karl G. Jansky Very Large Array in the radio (5 GHz), and with the 4.2 m William Herschel Telescope in the near-infrared and optical. Photometry was performed in the K_s, H, and J filters using the Long-slit Intermediate Resolution Infrared Spectrograph in imaging mode, and in the i', r', and g' filters with the auxiliary port camera. Ultraviolet observations were taken with the Ultraviolet Optical Telescope (P. W. A. Roming et al. 2005) on the Neil Gehrels Swift Observatory (N. Gehrels et al. 2004) in the *uvw*1, *uvm*2, and *uvw*2 filters. Finally, X-ray observations were taken with Chandra, using the Advanced CCD Imaging Spectrometer (ACIS; G. P. Garmire et al. 2003). The Chandra observations placed XTE J1118+480 at the aimpoint of the ACIS-S3 chip, and in assembling our SED, the X-ray data are included as a folded spectrum from 0.5 to 7 keV. P15 also supplemented their SED with nonsimultaneous infrared observations from the Spitzer Space Telescope and Wide-field Infrared Survey Explorer.

Table 1
Synchrotron Self-Compton– and Synchrotron-dominated Best-fit Parameters from MNW05 and BHJet

	P15 (MNW05)		This work (BHJet)	
Parameter (Unit)	SSC Fit	Synchrotron Fit	SSC Fit	Synchrotron Fit
$M_{\rm BH}$ ($M_\odot$)[a]	7.5	7.5	7.5	7.5
$D_{\rm lum}$ (kpc)	1.72	1.72	1.72	1.72
$\theta_{\rm i}$[a]	68°	68°	68°	68°
$f_{\rm nth}$ (percent)	60	60	10	10
$T_{\rm bb}$ (K)	3400	3400	3400	3400
R_* ($R_\odot$)	0.56	0.56	⋯	⋯
$L_{\rm bb}$ (10^{32} erg s^{-1})[b]	⋯	⋯	1.45	1.45
$N_{\rm j}$ ($10^{-5}L_{\rm Edd}$)	$1.71^{+1.52}_{-0.81}$	$2.67^{+4.54}_{-1.86}$	$0.32^{+0.09}_{-0.07}$	$59.38^{+46.04}_{-29.68}$
$\beta_{\rm p}$[c]	23^{+7}_{-12}	$0.48^{+0.44}_{-3.71}$	$1.3^{+0.6}_{-0.4}$	$0.005^{+0.011}_{-0.004}$
r_0 ($r_{\rm g}$)[d]	$2.3^{+1.2}_{-0.6}$	2.7 ± 0.9	2.1 ± 0.5	2.2 ± 0.3
$k_{\rm B}T_e$ (keV)[e]	1495^{+709}_{-360}	$709.0^{+19.7}_{-331.9}$	1642^{+436}_{-318}	135^{+64}_{-32}
$f_{\rm sc}$[f]	$<1.3 \times 10^{-6}$	2.5×10^{-3}	2.0×10^{-7}	1.0×10^{-4}
$z_{\rm diss}$ ($r_{\rm g}$)	14.4	20.2	50	50
s[g]	2.2	3	2	2
f_β[h]	⋯	⋯	0.04	<0.07
$f_{\rm pl}$	⋯	⋯	$-1.4^{+0.7}_{-0.8}$	$8.9^{+2.9}_{-4.3}$
$f_{\rm heat}$	⋯	⋯	1	1
χ^2_rc/dof[i]	0.59/28	0.54/29	0.82/27	0.51/27

Notes. Parameter values with uncertainties were fit by the model as free parameters, and values without uncertainties were kept frozen during the fitting. Cells filled with ⋯ mean that analogous free parameters do not exist between the two models. All model parameters are defined in Section 2.
[a] Following P15, we fixed the black hole mass to $M_{\rm BH} = 7.5\,M_\odot$and the orbital inclination to $\theta_{\rm i} = 68°$ (J. Khargharia et al. 2013).
[b] For consistency with P15, we froze the companion star luminosity to the equivalent value for a blackbody with the same temperature and radius adopted by P15.
[c] The equipartition ratio from L22, $\beta_{\rm p}$, is defined as the reciprocal of k in the MNW05 model ($k = U_B/U_e = 1/\beta_{\rm p}$ with $U_B = B^2/8\pi$). For convenience, we converted the k values reported by P15 to $\beta_{\rm p}$. For our new synchrotron fit we report formal statistical uncertainties, but we note that $\beta_{\rm p}$ is essentially an upper limit (<0.016).
[d] $r_{\rm g} = GM_{\rm BH}/c^2$ is the gravitational radius.
[e] Electron temperature is denoted as T_e in P15.
[f] Different nomenclature is adopted for this parameter between the two models: $\epsilon_{\rm sc}$ in Equation (1) of P15 is defined the same as $f_{\rm sc}$ in Equation (57) in L22.
[g] The parameter for the power-law index is denoted by p in P15.
[h] f_β was left as a free parameter, but its uncertainties left it essentially unconstrained in the SSC fit and provided only an upper limit in the synchrotron fit.
[i] Chi-squared over the degrees of freedom (dof).

3.2. Model Fitting

We fit the BHJet model to the broadband spectrum using the Interactive Spectral Interpretation System (ISIS; J. C. Houck & L. A. DeNicola 2000), which allows the best model fit to be determined through the minimization of the χ^2 statistic via least squares fitting. ISIS also forward folds the model through the X-ray response during the fitting process. Following P15, extinction corrections were applied to the near-infrared, optical, and ultraviolet data prior to fitting (see Table 1 of P15), and a fixed X-ray column density of $N_{\rm H} = 1.2 \times 10^{20}\,{\rm cm}^{-2}$ (J. E. McClintock et al. 2003) was applied to the X-ray data within ISIS during the fitting process.

We started with the agnjet flavor of BHJet, since the pressure-driven expansion is more analogous to the jet dynamics in the MNW05 model. We attempted fits with both the isothermal and adiabatic versions of agnjet, and we then moved onto the bljet flavor of BHJet. For all model flavors, we froze system parameters with observational constraints to the values adopted by P15, as listed in Table 1 (i.e., the black hole mass, inclination angle, companion star temperature, distance to the source, and so on).[8] Notably, C. A. Haswell et al. (2002) suggest a lower mass ($7\,M_\odot$) and slightly higher $T_{\rm bb}$ for the companion star. This difference of a few hundred kelvin would result in a shifted peak frequency, but we found that such a shift did not result in a significant difference in parameter fits. We therefore adopted the same blackbody temperature as P15 to ease comparison between the two models. Other parameters were left free.

To explore full parameter spaces, we started all fits by (manually) finding different sets of parameters that provided adequate fits (by eye), which resulted in around half a dozen initializations. For each initial guess, we then minimized χ^2 to find an initial fit (i.e., using the fit command in ISIS). Finally, we ran conf_loop to compute 68% confidence intervals on all free parameters, which adjusts each free parameter to determine the confidence interval based on $\Delta\chi^2$. If a better fit was found during this process, the best-fit parameters were updated and the confidence interval search started over from the improved parameters, thus minimizing the risk of converging to local minima. We found that three free parameters were always left essentially unconstrained, as judged by their large confidence intervals: $f_{\rm sc}$ (which controls the particle acceleration rate), $z_{\rm diss}$ (which controls the location of acceleration zone), and s (the power-law index of accelerated particles). Therefore, we performed a final fit (and run of conf_loop) where we fixed these three parameters to their best-fit values to minimize degeneracies with other parameters.

Through the above methodology, our set of around half a dozen initial guesses eventually converged to two different fits.

[8] To normalize the blackbody component from the companion star, P15 fixed the radius of the companion star to $0.56\,R_\odot$. In BHJet, this normalization is determined by the luminosity of the secondary, which we froze to 1.45×10^{32} erg s^{-1}, which is the luminosity of a spherical 3400 K blackbody with a radius of $0.56\,R_\odot$.

Similar to P15, one has X-ray emission dominated by SSC and the other by synchrotron radiation. Note, while we use χ^2 to guide our fitting, a successful fit is also judged by other factors including flat residuals of the data relative to the model, sensible physical parameters reported by the model, consistency with independent observations and analyses, and so forth. In particular, we pay attention to $\eta = n_e/n_p$ (the number density of electrons n_e to protons n_p) and require it not to become exceptionally large, nor do we allow a charged jet (i.e., $\eta < 1$).

4. Results

We found only the isothermal version of the `agnjet` model provided adequate fits (which is akin to the classical R. D. Blandford & A. Königl 1979 compact jet; also see Section 2.2). The adiabatic version of `agnjet` tended to predict highly inverted radio spectra, such that we struggled to self-consistently explain both the high- and low-energy emission. Ultimately, we found two different final fits with the `agnjet` model, one that explains X-ray emission as SSC from the thermal preacceleration zones, and a second fit that explains X-ray emission as synchrotron radiation from the nonthermal electrons in the acceleration zone (Figure 1). The best-fit parameters are presented in Table 1.

Among the most significant differences between the SSC and synchrotron fits is that the SSC fit prefers an equipartition factor close to unity ($\beta_p = 1.3$), while the synchrotron fit suggests that the magnetic energy dominates over the internal energies ($\beta_p < 0.016$).[9] The synchrotron fit also requires a much lower electron temperature of 135 keV in the jet base (versus 1642 keV for the SSC fit), and a significantly larger f_{sc} parameter (1.0×10^{-4} for the synchrotron fit versus 2.0×10^{-7} for the SSC fit; recall that this parameter is directly proportional to the particle acceleration rate). Both R. M. T. Connors et al. (2017) and D. Kantzas & F. Calore (2024) found synchrotron components to the X-ray emission from SED fits to the quiescent BHXRB A0620–00; however, their electron temperatures far exceed that of our synchrotron fit. This discrepancy could be reflecting physical differences between XTE J1118+480 and A0620–00. Or it could be systematic and explained by their lack of ultraviolet observations for constraining the preshock electron temperature. Indeed, we repeated our synchrotron-dominated fit to XTE J1118+480 after excluding our ultraviolet data points, and we found a higher (and uncertain) electron temperature of $k_B T_e = 3659^{+2414}_{-1402}$ keV. As noted in Section 3, the above values of f_{sc} are not highly constrained. However, in our initial exploration of parameter spaces, the synchrotron fit always required $f_{sc} > 10^{-5}$ to converge to any reasonable fit, while such high values could not reproduce reasonable SSC fits. In a sense, the dominant X-ray emission mechanism depends on f_{sc}: a higher f_{sc} enforces a higher maximum electron Lorentz factor, and the nonthermal synchrotron emission can extend to the X-rays. In contrast, a low f_{sc} will do the opposite.

We also note that the jet normalization, N_j, and the f_{pl} parameter (which controls the temperature profile of the postshock jet) are larger for the synchrotron fit compared to the `BHJet` SSC fit. It is also worth commenting that a consequence of the large N_j and low β_p in the synchrotron fit is a relatively mild pair load ($\eta = 6$), as calculated by `BHJet`. The SSC fit has a much larger $\eta = 105$. As seen in M. Lucchini et al. (2021b), the ratio of electron–positron pairs and protons ~20 is considered "mild" or "moderate." For the case of hard states in Z. Cao et al. (2022) the number ratio was forced to be ~30 to keep a reasonable energy budget and a jet power approximately on the order of the accretion disk luminosity. Therefore, we do not have cause to reject a fit on the grounds of a larger η, but we still wish to draw attention to it.

[9] We note that we explored solutions with the jet base in strict equipartition (by freezing $\beta_p = 1$) and could not find an adequate fit.

4.1. `bljet`

We also explored the `bljet` flavor of `BHJet`. When using `bljet` we set the terminal Lorentz factor γ_{acc} to two, which is reached at the location of the acceleration zone z_{acc} (we found higher terminal Lorentz factors did not provide acceptable fits). However, even with this low setting, the `bljet` model provided inadequate fits in our exploration of its parameter space. We could not replicate a fit with SSC dominating the X-ray emission, likely because of the highly magnetized jet base, which makes modeling bright SSC emission in objects with low mass accretion rates difficult.

On the other hand, `bljet` did converge to a version with synchrotron-dominated X-rays, with parameter values largely similar to the best-fit values we found with the `agnjet` model flavor. However, the resulting `bljet` fit had a highly magnetic jet base (i.e., a low equipartition factor β_p) that led to pair contents <1, thus producing a charged jet. We thus do not discuss `bljet` further.

5. Discussion

Below we discuss the SSC and synchrotron fits, including comparisons to each other and to P15. From a purely statistical perspective, it is challenging to argue that one fit is of better quality than the other. The residuals are slightly flatter in the synchrotron fit, especially from the infrared through ultraviolet. However, the synchrotron fit has a reduced $\chi^2_\nu = 0.51$, and a value <1 could suggest "overfitting" the data. Meanwhile, the SSC fit has a $\chi^2 = 0.82$, which is closer to unity (although could also suggest overfitting). For reasons discussed below, we tend to favor the SSC fit, implying that the X-ray emission is primarily produced by thermal distributions of (mildly) relativistic particles.

5.1. Synchrotron Self-Compton–dominated Fit

One of the reasons that P15 preferred their SSC fit with the MNW05 model is that their synchrotron fit required a low electron temperature in the jet base. Also, the postacceleration synchrotron radiation (from nonthermal particles) had a steep spectrum ($f_\nu \propto \nu^{-1}$) that was indicative of radiative cooling, even though radiative losses were not modeled by MNW05.

Despite being their preferred model, P15 did have one major criticism of their SSC fit. Namely, their SSC fit required the jet base to be out of equipartition, with less of the energy distributed into the magnetic field (P15 found $\beta_p = 23^{+7}_{-12}$). While there is no actual requirement that the base must be close to equipartition (even though equipartition is a common assumption in jet modeling), P15 could not provide a physical explanation for why the jet base in quiescence should be so magnetically weak. This is no longer a concern with `BHJet`, which found $\beta_p = 1.3^{+0.6}_{-0.4}$.

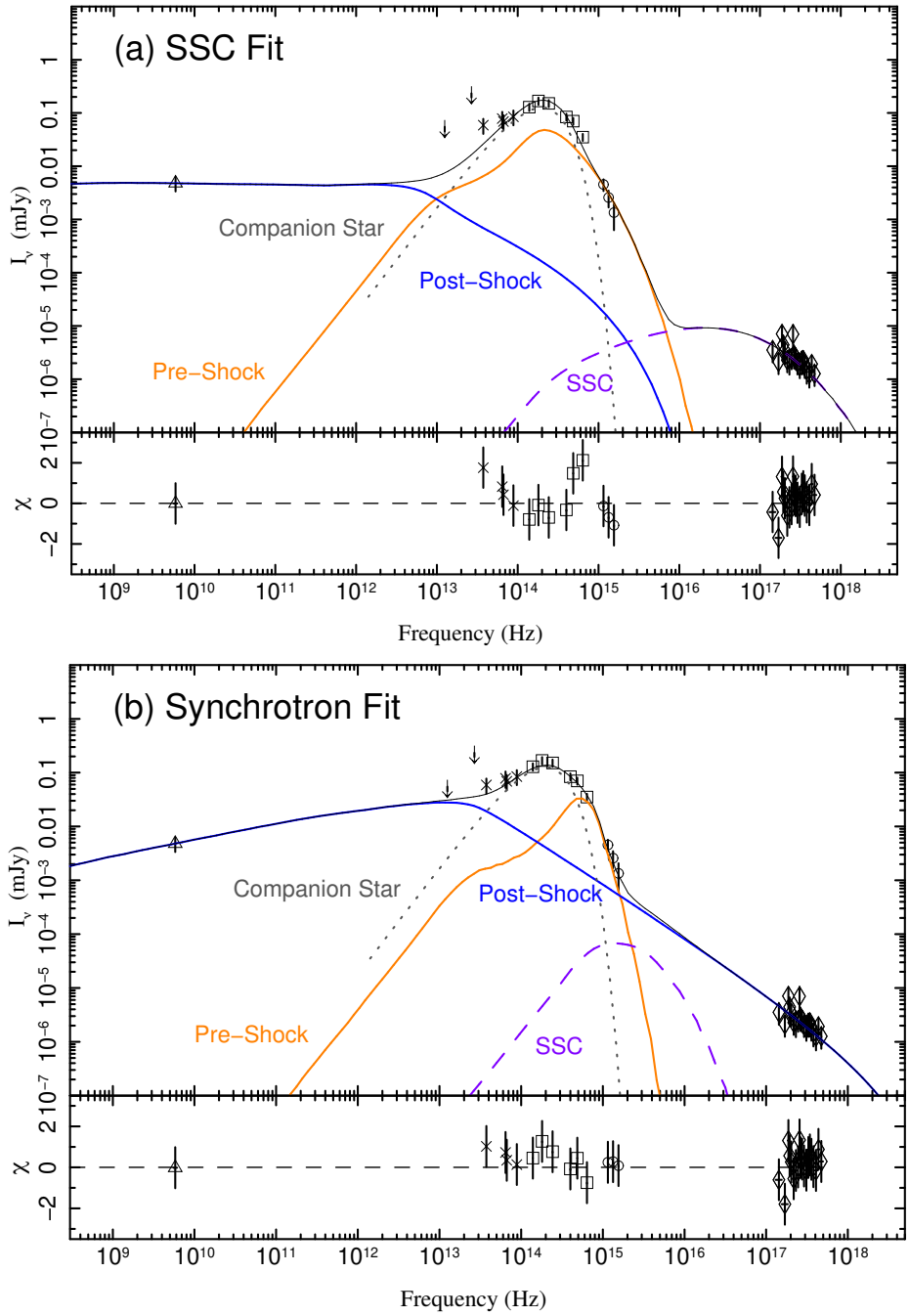

Figure 1. (a) `BHJet` model fit to the multiwavelength SED with X-rays dominated by SSC (panel (a)) and by synchrotron radiation (panel (b)). Depicted by shapes are radio (triangle), infrared (upper limits given by arrows, detections as crosses), near-infrared–optical (squares), ultraviolet (circles), and X-rays (diamonds). The best fit is shown as the black line with contributions from the preshock synchrotron emission (solid orange), companion star (dotted gray), postshock synchrotron emission (solid blue), and SSC (dashed purple). Residuals are shown in the bottom of each panel.

After the above difference in equipartition between the SSC fits from the MNW05 and `BHJet` models, the second biggest difference is that `BHJet` places the acceleration zone, $z_{\rm diss}$, 3.5 times farther from the black hole than the MNW05 model, which puts the jet break from 10^{12} to 10^{13} Hz (compared to 10^{13}–10^{14} Hz with the MNW05 model). However, $z_{\rm diss}$ is not well constrained by either model, since we do not have observational constraints on the location of the jet break for XTE J1118+480 in quiescence. Therefore, we cannot assess whether or not the larger distance ($z_{\rm diss}$) and higher jet break frequency represent an improvement over P15. However, we note that the introduction of (dominant) radiative cooling losses in `BHJet` effectively suppresses emission from optically thin regions, changing the power-law slope, s, of the radiating particles and thereby permitting small $z_{\rm diss}$ distances to be explored more physically.

Otherwise, the best-fit parameters from the `BHJet` SSC fit are generally comparable to the values obtained by MNW05 (see Table 1). In particular, the electron temperature, T_e, and the radius of the nozzle, r_0, are similar. This supports the conclusion from P15 that as BHXRBs fade from the hard state to quiescence, their jet bases become cooler and more compact (also see R. M. T. Connors et al. 2017). During state transitions at much higher Eddington ratios, X-ray coronae

(and/or jet bases) have been observed to change their sizes (e.g., E. Kara et al. 2019; J. Wang et al. 2021; Z. Cao et al. 2022; M. Méndez et al. 2022). We thus expect that the (thermal) jet base and/or corona evolve with the Eddington ratio during BHXRB outbursts. Note that P15 also suggested that the jet base becomes less magnetically dominated in quiescence, which our study now rejects.

In addition to a jet base being closer to equipartition, the other new insight gleaned from the BHJet model is that we infer low amounts of electron diffusion through the parameter f_β. However, we do not draw strong conclusions on the electron diffusion, since f_β is not well constrained in the SSC fit, and the parameter f_β is designed to absorb physical uncertainties in electron diffusion.

Finally, we cannot ignore that the SSC fit from BHJet suggests a relatively large η of 105 (ratio of lepton density to proton density). Considering, e.g., G. Ghisellini & F. Tavecchio (2010), the relativistic jet power will depend on the number of leptons and protons within the jet. G. Ghisellini & F. Tavecchio (2010) developed a method for approximating minimum jet powers for blazars, assuming there are no cold leptons, and they present an approximate upper bound on the ratio of electron–positron pairs per proton of $\sim$10. However, we stress that the blazars considered by G. Ghisellini & F. Tavecchio (2010) were at high accretion rates, and their modeling included seed photons from the blazar torus and broad-line region that inverse-Compton scatter off the jet, causing strong jet deceleration. Thus, their limit of $\eta < 10$ may not be applicable to a quiescent system like XTE J1118+480 that has a much lower accretion rate, and that lacks an analogous torus or broad-line region. For this reason, we take this estimate for positron pairs per proton as an order-of-magnitude constraint. One factor still not modeled in BHJet is the contribution of high-energy emission produced by pair annihilation. The SED of XTE J1118+480 does not include gamma-ray radiation: either it produces none, or is so faint in gamma rays as to remain undetectable. However, with a high $\eta = 105$, we might expect an increase in annihilation, and thus a spike in gamma rays. Inclusion of this effect into future versions of BHJet would help determine if $\eta = 105$ is on the right order of magnitude, or if it veers too high, particularly given recent advances in our ability to detect gamma rays from BHXRBs (LHAASO Collaboration et al. 2025).

5.2. Synchrotron-dominated Fit

Statistically, the synchrotron fit appears to be a reasonable representation of the data, but for several reasons we are skeptical if it provides an accurate physical interpretation. First, getting BHJet to converge to the synchrotron fit was predicated on assuming a large particle acceleration rate, by requiring $f_{\rm sc} > 10^{-5}$. We do not have observational constraints to inform if this is a reasonable assumption or not, but it is possibly concerning that the fit is so sensitive to this initial choice.

Once the large $f_{\rm sc}$ was frozen, the synchrotron fit then converged toward lower electron temperatures ($k_{\rm B}T_e = 135$ keV) and equipartition factors ($\beta_{\rm p} < 0.016$). Although this temperature better coincides with a classical corona temperature (e.g., T. Miyakawa et al. 2008; E. Kara & J. García 2025), a concerning consequence was that a larger jet power ($N_{\rm j} \sim 6 \times 10^{-4} L_{\rm Edd}$) was then required to supply enough electrons to produce a sufficiently high synchrotron radiation luminosity within a magnetically dominated environment. We expect any discrepancy between $N_{\rm j}$ and the "true" jet power to only be a factor of 2–3 (P. Crumley et al. 2017). Thus, a jet power of $6 \times 10^{-4} L_{\rm Edd}$ may simply be too large for a quiescent source, since it would imply an accretion power around that order of magnitude.[10]

Finally, further arguments against synchrotron-dominated X-rays are provided by P15 when considering the path XTE J1118+480 takes in the radio–X-ray luminosity plane as it ends an outburst. As the accretion rate drops in the inner accretion flow of hard state and quiescent BHXRBs, radio and X-ray luminosities decrease in tandem, following a nonlinear correlation (for XTE J1118+480, this is measured as $L_{\rm R} \propto L_{\rm X}^{0.7}$ over 5 decades in $L_{\rm X}$; E. Gallo et al. 2014). If X-ray emission is synchrotron cooled (see Section 5.3), then the correlation should steepen to $L_{\rm R} \propto L_{\rm X}^{1.2}$ (F. Yuan & W. Cui 2005), which is not observed. We refer the reader to Section 5.1 of P15 for additional details. Here, we simply comment that, since publication of P15, arguments against synchrotron-cooled X-rays from quiescent BHXRBs have become stronger, based on the lack of steep correlation slopes from two well-monitored BHXRB decays, the 2015 decay of V404 Cygni (R. M. Plotkin et al. 2017) and the 2018 decay of MAXI J1820+070 (A. W. Shaw et al. 2021).

5.3. The Addition of Radiative Losses in BHJet

We conclude our discussion by illustrating how the addition of radiative cooling losses in BHJet improves our modeling. Figure 2 compares the acceleration rate in the acceleration zone ($t_{\rm acc}^{-1}$) to the balance of energy losses due to synchrotron radiative cooling ($t_{\rm rad}^{-1}$) and adiabatic escape ($t_{\rm ad}^{-1}$). Except for the smallest Lorentz factors, we find that cooling is dominated by radiative losses, contrary to the assumption for adiabatic escape in MNW05. We believe this is a major reason that our SSC fit provides a more reasonable equipartition factor than the SSC fit published by P15.

We used the synchrotron-dominated fit to help illustrate the importance of including these radiative losses (even if we believe this fit to be less physical). We could only obtain a synchrotron fit with the BHJet model if we kept the power-law index of nonthermal particles close to $s = 2$. For $s = 2$, optically thin synchrotron radiation has a spectral index of -0.5 ($f_\nu \propto \nu^\alpha$). Yet, in our synchrotron fit we measure $\alpha = -1$ from the optical through soft X-ray (measured by fitting a power law to the synchrotron spectrum in Figure 1(b)), which is indicative of synchrotron-cooled X-rays. Between the jet break and the X-ray wave band, there is no additional break in the spectrum akin to a synchrotron cooling break (where the spectrum would steepen from $\alpha = -0.5$ to -1). Meaning, synchrotron radiation emerges from the jet break already cooled. In P15, where radiative losses were not included, the spectral index needed to be artificially frozen to $s = 3$ to replicate this behavior.

[10] We stress that the above arguments apply only to this particular fit of XTE J1118+480 in quiescence and are not a general statement on the agnjet flavor of BHJet. See, e.g., Section 7.2 L22, where an agnjet fit to the supermassive black hole M81* can produce a physically believable synchrotron fit.

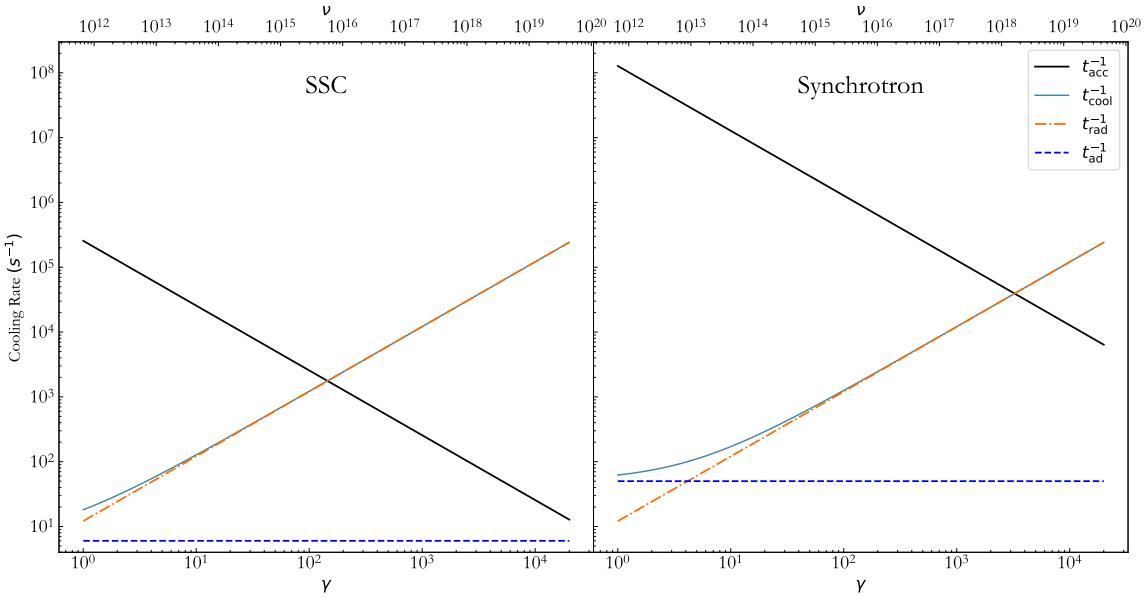

Figure 2. Cooling loss components for both the SSC fit (left) and the synchrotron fit (right) along with the acceleration rate, $t_{\rm acc}^{-1}$ (solid black line), plotted against observed frequency, ν, and Lorentz factor, γ. The total cooling rate, $t_{\rm cool}^{-1}$ (solid cyan line), is the sum of energy losses due to synchrotron emission, $t_{\rm rad}^{-1}$ (dashed–dotted orange line), and adiabatic escape losses, $t_{\rm ad}^{-1}$ (dashed blue line), and the cooling rate is dominated by synchrotron cooling losses.

6. Summary

We applied the multizone jet model, `BHJet`, to the SED of the high Galactic latitude BHXRB XTE J1118+480 in quiescence. We then compared our results to P15, who fit the same data using the earlier-generation MNW05 jet model. We found model fits that can explain the X-ray emission as either SSC from the preacceleration zone, or as synchrotron-cooled radiation from the acceleration zone. However, we argue that the SSC-dominated fit is more realistic, which implies that X-rays are dominated by radiation from a thermal population of particles.

Our work supports previous suggestions that quiescent BHXRBs have more compact and cooler jet bases in quiescence (P15; R. M. T. Connors et al. 2017), but we reject the claim from P15 that the jet base is less magnetically dominated in quiescence. We also discuss that the inclusion of radiative losses in `BHJet` is a significant improvement. At the moment, only two known quiescent BHXRBs with very low Eddington ratios ($L_{\rm X}/L_{\rm Edd} \sim 10^{-8.5}$) have sufficiently high fluxes to allow this type of broadband modeling. The discovery of new, nearby quiescent BHXRBs (ideally with low line-of-sight absorption) is essential to eventually understand if the results obtained for XTE J1118+480 are representative of the entire quiescent BHXRB population.

Acknowledgments

O.D.C. acknowledges support from NASA under award No 80NSSC23M0104. R.M.P. acknowledges support from the National Science Foundation under grant No. 2511711. We thank the anonymous referee for helpful comments that improved this manuscript.

Software: `Astropy` (Astropy Collaboration et al. 2013, 2018, 2022), `BHJet` (M. Lucchini et al. 2021a), `ISIS` (J. C. Houck & L. A. DeNicola 2000).

ORCID iDs

Octavia D. Clapp https://orcid.org/0000-0002-3260-3960
Richard M. Plotkin https://orcid.org/0000-0002-7092-0326
Matteo Lucchini https://orcid.org/0000-0002-2235-3347
Sera Markoff https://orcid.org/0000-0001-9564-0876
Elena Gallo https://orcid.org/0000-0001-5802-6041
Zihao Zuo https://orcid.org/0009-0000-8524-8344

References

Astropy Collaboration, Robitaille, T. P., Tollerud, E. J., et al. 2013, A&A, 558, A33
Astropy Collaboration, Price-Whelan, A. M., Sipőcz, B. M., et al. 2018, AJ, 156, 123
Astropy Collaboration, Price-Whelan, A. M., Lim, P. L., et al. 2022, ApJ, 935, 167
Belloni, T. M., & Motta, S. E. 2016, ASSL, 440, 61
Bernardini, F., & Cackett, E. M. 2014, MNRAS, 439, 2771
Blandford, R. D., & Königl, A. 1979, ApJ, 232, 34
Borowski, E. S., Hynes, R. I., Hunt, Q., et al. 2025, ApJL, 991, L31
Cao, Z., Lucchini, M., Markoff, S., Connors, R. M. T., & Grinberg, V. 2022, MNRAS, 509, 2517
Carotenuto, F., Corbel, S., & Tzioumis, A. 2022, MNRAS, 517, L21
Connors, R. M. T., Markoff, S., Nowak, M. A., et al. 2017, MNRAS, 466, 4121
Corbel, S., Tomsick, J. A., & Kaaret, P. 2006, ApJ, 636, 971
Corbel, S., Coriat, M., Brocksopp, C., et al. 2013, MNRAS, 428, 2500
Crumley, P., Ceccobello, C., Connors, R. M. T., & Cavecchi, Y. 2017, A&A, 601, A87
Crumley, P., Caprioli, D., Markoff, S., & Spitkovsky, A. 2019, MNRAS, 485, 5105
dePolo, D. L., Plotkin, R. M., Miller-Jones, J. C. A., et al. 2022, MNRAS, 516, 4640
Dinçer, T., Bailyn, C. D., Miller-Jones, J. C. A., Buxton, M., & MacDonald, R. K. D. 2018, ApJ, 852, 4
Dzib, S. A., Massi, M., & Jaron, F. 2015, A&A, 580, L6
Esin, A. A., McClintock, J. E., & Narayan, R. 1997, ApJ, 489, 865
Esin, A. A., McClintock, J. E., Drake, J. J., et al. 2001, ApJ, 555, 483
Falcke, H., & Markoff, S. 2000, A&A, 362, 113
Fender, R. 2010, in Lecture Notes in Physics, ed. T. Belloni, Vol. 794 (Springer), 115
Gallo, E., Fender, R. P., & Hynes, R. I. 2005, MNRAS, 356, 1017
Gallo, E., Fender, R. P., Miller-Jones, J. C. A., et al. 2006, MNRAS, 370, 1351

Gallo, E., Migliari, S., Markoff, S., et al. 2007, ApJ, 670, 600
Gallo, E., Miller-Jones, J. C. A., Russell, D. M., et al. 2014, MNRAS, 445, 290
Garmire, G. P., Bautz, M. W., Ford, P. G., Nousek, J. A., & Ricker George, R. J. 2003, SPIE, 4851, 28
Gehrels, N., Chincarini, G., Giommi, P., et al. 2004, ApJ, 611, 1005
Gelino, D. M., Balman, Ş., Kızıloğlu, Ü., et al. 2006, ApJ, 642, 438
Ghisellini, G., & Tavecchio, F. 2010, MNRAS, 409, L79
Haswell, C. A., Hynes, R. I., King, A. R., & Schenker, K. 2002, MNRAS, 332, 928
Houck, J. C., & DeNicola, L. A. 2000, ASPC, 216, 591
Hynes, R. I., Charles, P. A., Garcia, M. R., et al. 2004, ApJL, 611, L125
Hynes, R. I., Bradley, C. K., Rupen, M., et al. 2009, MNRAS, 399, 2239
Ichimaru, S. 1977, ApJ, 214, 840
Kantzas, D., & Calore, F. 2024, A&A, 690, A87
Kara, E., & García, J. 2025, ARA&A, 63, 379
Kara, E., Steiner, J. F., Fabian, A. C., et al. 2019, Natur, 565, 198
Khargharia, J., Froning, C. S., Robinson, E. L., & Gelino, D. M. 2013, AJ, 145, 21
Kong, A. K. H., McClintock, J. E., Garcia, M. R., Murray, S. S., & Barret, D. 2002, ApJ, 570, 277
LHAASO Collaboration, Cao, Z., Aharonian, F., et al. 2025, NSRev, 12, nwaf496
Lucchini, M., Ceccobello, C., Markoff, S., et al. 2021a, BHJet: Semi-analytical black hole jet model, Astrophysics Source Code Library, ascl:2109.024
Lucchini, M., Russell, T. D., Markoff, S. B., et al. 2021b, MNRAS, 501, 5910
Lucchini, M., Ceccobello, C., Markoff, S., et al. 2022, MNRAS, 517, 5853
Maitra, D., Markoff, S., Brocksopp, C., et al. 2009, MNRAS, 398, 1638
Malzac, J., Merloni, A., & Fabian, A. C. 2004, MNRAS, 351, 253
Markoff, S. 2010, LNP, 794, 143
Markoff, S., Falcke, H., & Fender, R. 2001, A&A, 372, L25
Markoff, S., Nowak, M., Corbel, S., Fender, R., & Falcke, H. 2003, NewAR, 47, 491
Markoff, S., Nowak, M. A., & Wilms, J. 2005, ApJ, 635, 1203
Markoff, S., Nowak, M., Young, A., et al. 2008, ApJ, 681, 905
McClintock, J. E., Narayan, R., Garcia, M. R., et al. 2003, ApJ, 593, 435
Méndez, M., Karpouzas, K., García, F., et al. 2022, NatAs, 6, 577
Miyakawa, T., Yamaoka, K., Homan, J., et al. 2008, PASJ, 60, 637
Narayan, R., & Yi, I. 1994, ApJL, 428, L13
Narayan, R., & Yi, I. 1995, ApJ, 444, 231
Plotkin, R. M., Gallo, E., & Jonker, P. G. 2013, ApJ, 773, 59
Plotkin, R. M., Gallo, E., Markoff, S., et al. 2015, MNRAS, 446, 4098
Plotkin, R. M., Miller-Jones, J. C. A., Gallo, E., et al. 2017, ApJ, 834, 104
Plotkin, R. M., Miller-Jones, J. C. A., Chomiuk, L., et al. 2019, ApJ, 874, 13
Plotkin, R. M., Bahramian, A., Miller-Jones, J. C. A., et al. 2021, MNRAS, 503, 3784
Rana, V., Loh, A., Corbel, S., et al. 2016, ApJ, 821, 103
Remillard, R. A., & McClintock, J. E. 2006, ARA&A, 44, 49
Reynolds, M. T., Reis, R. C., Miller, J. M., Cackett, E. M., & Degenaar, N. 2014, MNRAS, 441, 3656
Ribó, M., Munar-Adrover, P., Paredes, J. M., et al. 2017, ApJL, 835, L33
Roming, P. W. A., Kennedy, T. E., Mason, K. O., et al. 2005, SSRv, 120, 95
Shakura, N. I., & Sunyaev, R. A. 1973, A&A, 24, 337
Shaw, A. W., Plotkin, R. M., Miller-Jones, J. C. A., et al. 2021, ApJ, 907, 34
Sironi, L., & Spitkovsky, A. 2011, ApJ, 726, 75
Torres, M. A. P., Callanan, P. J., Garcia, M. R., et al. 2004, ApJ, 612, 1026
Tremou, E., Corbel, S., Fender, R. P., et al. 2020, MNRAS, 493, L132
Veledina, A., Poutanen, J., & Vurm, I. 2011, ApJL, 737, L17
Vila, G. S., Romero, G. E., & Casco, N. A. 2012, A&A, 538, A97
Wang, J., Mastroserio, G., Kara, E., et al. 2021, ApJL, 910, L3
Yuan, F., & Cui, W. 2005, ApJ, 629, 408
Yuan, F., & Narayan, R. 2014, ARA&A, 52, 529
Yuan, F., Cui, W., & Narayan, R. 2005, ApJ, 620, 905
Yue, H., Zhang, J., Ge, Y., et al. 2026, ApJ, 997, 163
Zuo, Z., Cugno, G., Michail, J., et al. 2025, ApJ, 991, 157